Supporting Information

Whiteside et al. 10.1073/pnas.1001706107

SI Text

Evidence that These Molecules Originate Predominately from Indigenous Vascular Plants. The saturate fraction of extractions from multiple samples from the Hartford-Newark and St. Audrie's Bay section (Datasets S1 and S3) show an odd-over-even preference for the C_{25-31} *n*-alkanes, characteristic of an origin from vascular plant cuticular waxes (1). Further evidence of this origin is indicated by their high carbon preference index (CPI) and relatively low thermal alteration, consistent with published data that indicates that much of the Jurassic Newark–Hartford section in the upper part of the oil window and that the St. Audrie's section is thermally immature (Fig. S1 and Dataset S3). Newark and Hartford extractions generally have less obvious carbon preference, and some have CPIs characteristic of hydrocarbons generated from the organic matter (Fig. S1 and Dataset S1). Because of the very high Newark and Hartford basin accumulation rates, the relatively very small volumes of organic rich strata and the observed differences in *n*-alkane FID chromatograms and $\delta^{13}C$ values between samples only a few meters apart (Fig. S1), the Newark and Hartford $\delta^{13}C_{alk}$ values represent local, in situ hydrocarbons from indigenous organic matter. They are thus most simply interpreted as representative of the original *n*-alkane values. This is consistent with published thermal maturity data that indicate low thermal maturity ($R_0 = 0.4 - 1.0$; see refs. 2–4) of Newark and Hartford samples, just within the oil window.

Supporting Paleomagnetic Correlations. Hounslow et al. (5) document the presence of a thin reverse interval above the initial excursion (zone SA5r), with the rest of their postinitial sampled stratigraphy being of normal polarity. It is our contention that this reverse polarity zone should correlate to the section immediately above the Orange Mountain Basalt, but no reverse polarity zones were found in the Newark basin coring project sampling of that interval (lower Feltville Formation). Three lines of evidence lead us to argue they may have been missed by the initial sampling. First, the lower Feltville Formation is largely gray and black beds that were not sampled by Kent et al. (1995) because of their less favorable magnetic behavior compared to red beds, and thus most of the lower Feltville was not sampled. Second, the lower Feltville Formation in the Martinsville no. 1 core is highly condensed compared to elsewhere in the basin (Olsen et al., 1996a) and the reverse zone could easily be omitted. Third, two thin zones of reverse polarity have been identified in interbedded cyclical lacustrine strata and Central Atlantic magmatic province (CAMP) basalts of the Central High Atlas, Morocco (Knight et al., 2004) correlative to the lower Feltville Formation (Whiteside et al., 2007), and three thin zones of reverse polarity occur close to and above the extinction level in the Moncornet core in the Paris basin (6). Such stratigraphically thin polarity zones are easy to miss and difficult to interpret, but their presence in multiple sections leads us to interpret reverse polarity zone SA5r at St. Audrie's as correlative with one of the two, probably the upper, reverse zone in the Central High Atlas and one of the upper two in the Moncornet core. Additional sampling of eastern North American strata is underway to locate these polarity zones within the Newark and Fundy basin sections.

***n*-Alkane Data from Newark and Hartford Basins and St. Audrie's Bay.** For the Newark and Hartford basins (Datasets S1 and S2), the data are placed in the orbitally calibrated time scale of Whiteside et al. (7) and Kent and Olsen (8). Samples are registered into the detailed litho- and cyclostratigraphy from each basin section, for the most part based on core or long outcrop transects. A synthetic target climatic precession curve, described in ref. 7, was constructed using the values for *k* (precessional constant, from ref. 9) for the Late Triassic–Early Jurassic (approximately 200 Ma) and values of g3 and g4 (fundamental frequencies of Earth and Mars), derived from the empirical observations of the frequency of the beat cycle (g3–g4) of these frequencies visible in the Newark basin record (10). Inasmuch as there are infinite solutions to the g3–g4 equation for a single value (two variables and two unknowns), we use the average within the chaotic zone as defined by Laskar et al. (11), for the empirical value for g3–g4 of 1/1.75 m.y. (10), with amplitudes derived from ref, 12. The sections in the depth domain were then tuned to the target curve using the linage option of Analyseries (13) assuming that the peak values in depth ranks correspond to precessional maxima. The St Audrie's Bay data (Dataset S3) are placed within the depth scale of Ruhl et al. (14, 15).

CPI and Average Chain Length. CPI was calculated using a modified version of the "improved" (CPI2) method (16) using the following formula:

$$1/2([(A_{25}+A_{27}+A_{29})/(A_{26}+A_{28}+A_{30})] + [(A_{27}+A_{29}+A_{31})/(A_{26}+A_{28}+A_{30})]). \quad \textbf{[S1]}$$

Average chain length (ACL) was calculated using a formula modified from ref. 17as follows:

$$ACL = [(25^*A_{25}) + (27^*A_{27}) + (29^*A_{29}) + (31^*A_{31})]/(A_{25}+A_{27}+A_{29}+A_{31}). \quad \textbf{[S2]}$$

In both Eqs. **S1** and **S2**, A is the area under the chromatographic peak for each *n*-alkane of a specific chain length and for Eq. **S2**, 25, 27, 29, and 31 are the individual *n*-alkane chain lengths.

Additional Carbonate and Bulk Organic $\delta^{13}C$ Records. The $\delta^{13}C_{org}$ and $\delta^{13}C_{carb}$ patterns seen in the three marine sections shown in Fig, 2 of the main text are not limited to those localities. Here, we show seven other examples, all with consistent biological patterns at the extinction level (Fig. S2). These additional localities are Kuhjoch, Austria [the global stratotype section and point (GSSP) for the base Jurassic] (18, 19); Tiefengraben, Austria (20, 21); New York Canyon, Nevada (22); the Mingolsheim Core, Germany (23); and the Dorset Coast (24). We also provide new $\delta^{13}C_{org}$ data from the marine Blue Lias Formation at Lyme Regis, Dorset, England (collected by J.H.W.; see Table S1). The important feature to note is the initial excursion, similarity of the smaller positive excursion present at the higher resolution (St. Audrie's Bay, Kuhjoch, Tiefengraben, New York Canyon), and different degrees of a gradual positive excursion (Fig. S2) seen in the middle Hettangian in the long sections in both bulk organic and carbonate $\delta^{13}C$ (Lyme Regis, Mingolsheim, Dorset Coast, Kennecott Point, Val Adrara; refs. 23, 25) and seen in the Newark and Hartford data.

1. Eglinton G, Hamilton RJ (1967) Leaf epicuticular waxes. *Science* 156:1322–1335.
2. Spiker E, et al. (1988) Source of kerogen in black shales from the Hartford and Newark basins eastern United States. *US Geological Survey Bulletin* 1776:63–68.
3. Kotra RM, et al. (1988) Chemical composition and thermal maturity of kerogen and phytoclasts of the Newark Supergroup in the Hartford basin. *U.S. Geological Survey Bulletin* 1776:68–74.

4. Malinconico MAL (2002) Lacustrine organic sedimentation, organic metamorphism and thermal history of selected Early Mesozoic Newark Supergroup basins, Eastern U.S.A. PhD thesis (Department of Earth and Environmental Sciences, Columbia Univ, New York).
5. Hounslow MW, Posen PE, Warrington G (2004) Magnetostratigraphy and biostratigraphy of the Upper Triassic and lowermost Jurassic succession, St. Audrie's Bay, UK. *Palaeogeogr Palaeocl* 213:331–358.
6. Yang Z, et al. (1996) Hettangian and Sinemurian magnetostratigraphy from the Paris Basin. *J Geophys Res* 101:8025–8042.
7. Whiteside JH, et al. (2007) Synchrony between the CAMP and the Triassic-Jurassic mass-extinction event? *Palaeogeogr Palaeocl* 244:345–367.
8. Kent DV, Olsen PE (2008) Early Jurassic magnetostratigraphy and paleolatitudes from the Hartford continental rift basin (eastern North America): Testing for polarity bias and abrupt polar wander in association with the central Atlantic magmatic province. *J Geophys Res* 113:B06105, doi:10.1029/2007JB005407.
9. Berger AM, Loutre M, Laskar J (1992) Stability of the astronomical frequencies over the Earth's history for paleoclimate studies. *Science* 255:260–566.
10. Olsen PE, Kent DV (1999) Long-period Milankovitch cycles from the Late Triassic and Early Jurassic of eastern North America and their implications for the calibration of the early Mesozoic time scale and the long-term behavior of the planets. *Philos T R Soc A* 357:1761–1787.
11. Laskar J (1990) The chaotic motion of the solar system. A numerical estimate of the size of the chaotic zones. *Icarus* 88:266–291.
12. Laskar J, et al. (2004) A long-term numerical solution for the insolation quantities of the Earth. *Astron Astrophys* 428:261–285
13. Paillard D, Labeyrie L, Yiou P (1996) Macintosh program performs time-series analysis. *Eos Trans AGU* 77:379.
14. Ruhl M (2010) Carbon cycle changes during the Triassic–Jurassic transition. *Laboratory of Paleobotany and Palynology, Contribution Series 28* (Utrecht Univ, The Netherlands).
15. Ruhl M, et al. (2010) Astronomical constraints on the duration of the early Jurassic Hettangian stage and recovery rates following the end-Triassic mass extinction (St. Audrie's Bay/East Quantoxhead, UK). *Earth Planet Sci Lett* (in press).
16. Marzi R, Torkelson BE, Olson RK (1993) A revised carbon preference index. *Org Geochem* 20:1303–1306.
17. Smith FA, Wing SL, Freeman KH (2007) Magnitude of the carbon isotope excursion at the Paleocene–Eocene thermal maximum: The role of plant community change. *Earth Planet Sci Lett* 262:50–65.
18. Hillebrandt Av, Krystyn L, Kürschner WM (2008) A candidate GSSP for the base of the Jurassic in the Northern Calcareous Alps (Kuhjoch section, Karwendel Mountains, Tyrol, Austria). *Int. Subcomm. Jurassic Stratigr. Newslett.* 34:2–20.
19. Morton N (2008) Details of voting on proposed GSSP and ASSP for the base of the Hettangian Stage and Jurassic System. *Int Subcomm Jurassic Stratigr Newslett* 35:74.
20. Kürschner WM, Bonis NR, Krystyn L (2007) Carbon-isotope stratigraphy and palynostratigraphy of the Triassic–Jurassic transition in the Tiefengraben section Northern Calcareous Alps (Austria). *Palaeogeogr Palaeocl.* 244:257280.
21. Ruhl M et al. (2009) Triassic–Jurassic organic carbon isotope stratigraphy of key sections in the western Tethys realm (Austria). *Earth Planet Sci Lett* 281:169–187.
22. Guex J, et al. (2004) High-resolution ammonite and carbon isotope stratigraphy across the Triassic–Jurassic boundary at New York Canyon (Nevada). *Earth Planet Sci Lett* 225:29–41
23. van de Schootbrugge B, et al. (2008) Carbon cycle perturbation and stabilization in the wake of the Triassic–Jurassic boundary mass-extinction event *Geochem Geophys Geosy* doi: 10.1029/2007GC001914
24. Jenkyns HC, et al. (2002) Chemostratigraphy of the Jurassic System: Applications, limitations and implications for palaeoceanography *J Geol Soc London* 159:351–378.
25. Galli MT, et al. (2007) Stratigraphy and palaeoenvironmental analysis of the Triassic–Jurassic transition in the western Southern Alps (Northern Italy). *Palaeogeogr Palaeocl*. 244:52–70.

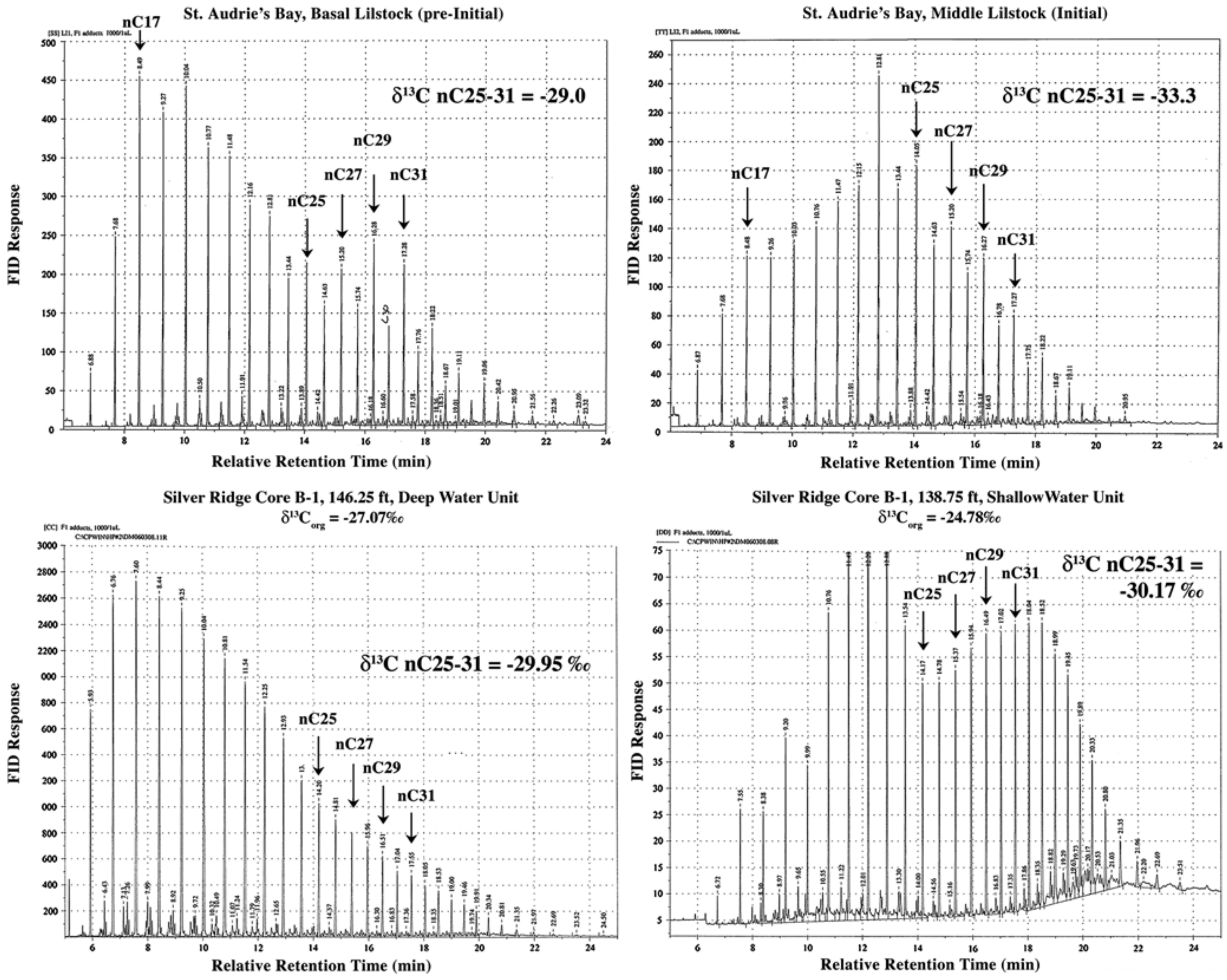

Fig. S1. Comparison between flame ion detector traces of samples from St. Audrie's Bay (above), and the Hartford basin (below) (from Dataset S1).

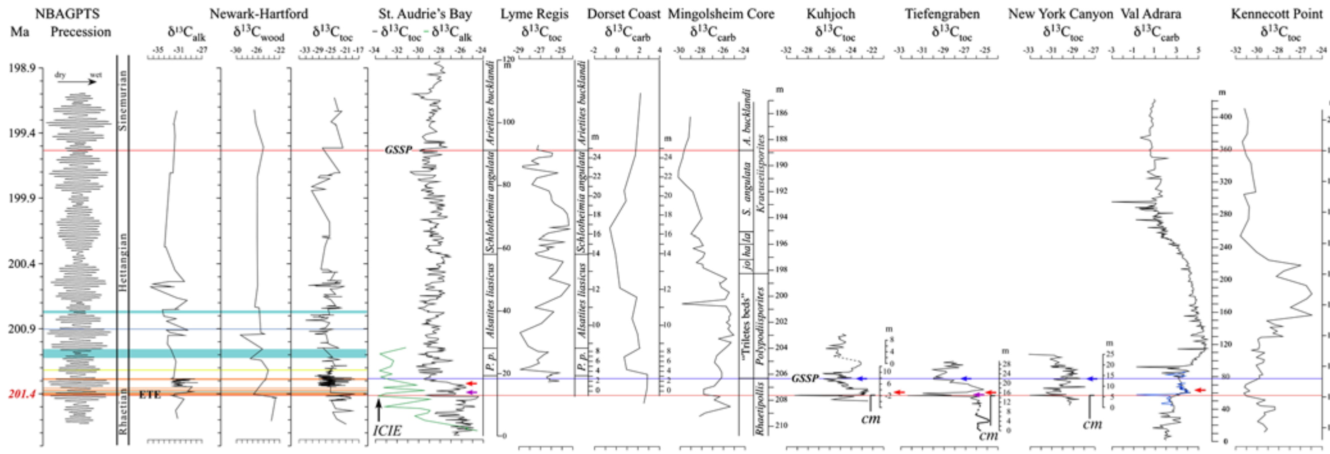

Fig. S2. Auxillary sections of $\delta^{13}C_{org}$ and $\delta^{13}C_{carb}$ from various localities compared to the Newark–Hartford, St. Audrie's Bay, and Kennecott Point and Val Adrara data. These are: Lyme Regis, Dorset, England (see Table S1); the Dorset Coast (24); Mingolsheim Core, Germany (23); Kuhjoch, Austria (the GSSP for the base Jurassic) (18); Tiefengraben, Austria (20); New York Canyon, Nevada (22); and Val Adrara, Italy (23). Red lines are the Hettangian–Sinemurian boundary above and the main extinction level below. The blue curve in the Val Adrara data is from ref. 25 added by ref. 23 to their data. The $\delta^{13}C_{carb}$ samples for Val Adrara are bulk carbonate, but those for the Dorset Coast are nonscreened oysters (24). All the short sections and St. Audrie's Bay were correlated following refs. 21 or 22. The other correlations are original. Black arrows point to the initial excursion; blue arrows indicate the position of the first appearance of the ammonite *Psiloceras spelae*, which has been picked as the taxon marking the base of the Jurassic at the newly identified GSSP (19) except at St. Audrie's Bay where it represents the correlative position of where it should occur based on ref. (21); red arrows mark the last appearance of *Rhaetipollis germanicus*; and purple arrows mark the last occurrence of conodonts. Abbreviations are BA, Blue Anchor Formation; buck Z, bucklandi Zone; *cm*, last occurence of the Triassic ammonite *Choristoceras*; *ha*, *P. hagenowi*; *jo*, *C. johnstoni*; L, Lilstock Formation; *la*, *A. laqueus*; *M*, main isotopic excursion; pla Z, planorbis Zone; Westb, Westbury Formation. Other symbols, colors, and notation as in main text Fig. 4.

Table S1. $\delta^{13}C_{org}$ data from Lyme Regis

Midpoints, m	$\delta^{13}C$	Sample identification number	Midpoints, m	$\delta^{13}C$	Sample identification number
0			14.70	-25.78	15.10.05.16
2.12	−26.26	15.10.05.50	14.80	−26.18	15.10.05.17
2.32	−25.18	15.10.05.51	14.95	−27.10	15.10.05.18
2.50	−26.18	15.10.05.52	15.25	−24.74	15.10.05.19
2.68	−26.10	15.10.05.a1	15.55	−27.19	15.10.05.20
2.85	−26.32	15.10.05.a2	15.85	−26.77	15.10.05.21
3.11	−26.43	15.10.05.a3 ss	16.15	−26.26	15.10.05.50
3.36	−26.10	15.10.05.A4	16.57	−24.24	15.10.05.23
3.54	−26.07	15.10.05.a5	16.73	−26.02	15.10.05.24
3.82	−25.19	17.10.05	16.92	−24.29	15.10.05.24b
4.45	−28.94	17.10.05.p3	17.59	−24.34	15.10.05.25
5.02	−27.92	17.10.05.p4	18.19	−24.45	15.10.05.26
5.63	−27.12	17.10.05.pb2	18.64	−24.83	15.10.05.27
6.21	−27.33	15.10.05.01	19.20	−25.64	15.10.05.28
7.20	−26.63	17.10.05.pb 2B	19.55	−25.93	15.10.05.29
7.59	−26.29	17.10.05.pb 2a	20.01	−25.99	15.10.05.30
7.75	−27.27	17.10.05.pb	20.56	−26.18	15.10.05.31
9.49	−28.97	15.10.05.02	21.22	−27.82	15.10.05.31
10.03	−26.92	15.10.05.03	21.87	−27.35	15.10.05.32
10.69	−25.73	15.10.05.04	22.41	−25.37	15.10.05.33
10.92	−27.53	15.10.05.5	22.85	−28.07	15.10.05.34
11.59	−25.02	15.10.05.06	23.01	−28.74	16.10.05.0
12.25	−24.16	15.10.05.07	23.14	−28.72	15.10.05.34B
12.61	−26.17	15.10.05.08	23.34	−27.17	15.10.05.35
12.95	−25.52	15.10.05.09	23.66	−27.85	16.10.05.01
13.59	−24.83	15.10.05.10	24.01	−27.21	15.10.05.36b
13.95	−27.38	15.10.05.11	24.16	−25.92	15.10.05.37
14.13	−27.51	15.10.05.12	24.46	−25.84	15.10.05.47
14.33	−26.72	15.10.05.13	24.81	−27.32	16.10.05.04
14.50	−26.17	15.10.05.14	25.08	−27.31	16.10.05.05
14.63	−26.45	15.10.05.15	25.33	−27.22	16.10.05.07

Other Supporting Information Files

Dataset S1 (XLS)
Dataset S2 (XLS)
Dataset S3 (XLS)